Diagnosis of the Surface Momentum Balance over the Tropical Pacific Ocean

CLARA DESER

Cooperative Institute for Research in Environmental Sciences, University of Colorado, Boulder, Colorado

(Manuscript received 26 April 1991, in final form 19 April 1992)

ABSTRACT

The purpose of this study is to evaluate the suitability of using linear drag as a proxy for surface friction in the observed climatological-mean momentum balance over the tropical Pacific Ocean. The linear drag parameterization of kinetic energy dissipation in the planetary boundary layer is widely used in simplified models of the tropical atmosphere, and in numerous observational studies of the surface momentum balance. Climatological seasonal-mean fields of sea level pressure and surface wind from the Comprehensive Ocean–Atmosphere Data Set are used to calculate the pressure gradient, Coriolis, and acceleration terms in the momentum budget; friction is derived as a residual. It is found that when friction is parameterized as a linear dissipation of kinetic energy, the damping time scale for the meridional wind is ~2–3 times faster than the damping time for the zonal wind. The preceding formulation fits the observations well, especially in the trade-wind regions. It is suggested that the different damping coefficients for the zonal (u) and meridional (v) winds are, in part, a reflection of the different vertical profiles of u and v in the planetary boundary layer.

A realistic simulation of the tropical surface wind field from the observed sea level pressure field is obtained using a linear momentum balance with unequal damping time scales for u and v. With equal damping times, the meridional component of the surface flow is too strong. Nonlinear advection improves the zonal wind simulation in limited regions of the northeast trades, equatorial easterlies, and off South America, but only by ~0.5 m s^{-1}.

1. Introduction

The surface wind field plays a crucial role in tropical air–sea interaction. Surface winds regulate sea surface temperatures by controlling the rate of air–sea energy exchange and mixing and advective processes in the upper ocean, while sea surface temperatures influence the low-level wind field and the distribution of atmospheric convection via surface fluxes. The surface wind field over the tropical oceans is determined primarily by a balance between the pressure gradient, Coriolis, and frictional forces (Gordon and Taylor 1975; Hastenrath and Lamb 1978; Egger et al. 1981; Murphree and van den Dool 1988; Zebiak 1990). The parameterization of surface friction is problematic and complex; in the studies just cited, friction is assumed to be adequately represented by linear drag, with a dissipation time scale on the order of 0.5–1 days. The purpose of this study is to test that assumption: how realistic is linear drag as a parameterization of surface friction for the observed climatological-mean winds over the tropical Pacific Ocean?

In a recent study, Murphree and van den Dool (1988) modeled the tropical surface wind field from observed climatological monthly mean sea level pressures using the nonlinear steady-state momentum equations. Dissipation was parameterized as linear damping and diffusion. Their zonal wind simulations were generally realistic: however, the meridional component of the trade winds was ~50% stronger than observed (see their Fig. 3c). Nonlinearity played only a minor role in the momentum balance.

Zebiak (1990) evaluated the terms in the vorticity budget for selected monthly surface wind anomaly fields over the tropical Pacific Ocean. He found that (a) the nonlinear advection terms are of second order, and (b) when surface friction is parameterized as linear damping, the residual term in the vorticity budget is first-order and resembles the stretching term. Although an assessment of data quality was not the main purpose of his study, Zebiak concluded from this result that the observed wind field contained data errors that were such as to artificially inflate the divergent component of the flow. This study will show that the excessive divergence and meridional flow in Zebiak's and Murphree and Van den Dool's simulations, respectively, result from their assumptions about the parameterization of surface friction.

2. Surface momentum balance

The surface momentum balance may be written as

$$\frac{d\mathbf{V}}{dt} + f\mathbf{k} \times \mathbf{V} = -\frac{1}{\rho}\nabla p + \frac{1}{\rho}\frac{\partial \boldsymbol{\tau}}{\partial z}$$

Corresponding author address: Dr. Clara Deser, CIRES, University of Colorado, Campus Box 449, Boulder, CO 80309.

where $\boldsymbol{\tau}$ is the vertical eddy stress term: $\tau^x = \overline{u'w'}$; $\tau^y = \overline{v'w'}$, and the other symbols have their conventional meanings. The eddy stress term arises because turbulent eddies transport horizontal momentum vertically: where the momentum flux converges (diverges), the mean flow will be accelerated (decelerated). The turbulent eddies transfer momentum from the atmospheric planetary boundary layer to the earth's surface, removing momentum from the boundary layer. A simple parameterization of the vertical eddy stress gradient at the surface is that it opposes the wind:

$$\frac{1}{\rho}\frac{\partial \boldsymbol{\tau}}{\partial z} = -\epsilon \mathbf{V}$$

where ϵ^{-1} is the apparent damping time scale for the surface wind. With this parameterization, the climatological-mean surface momentum balance becomes, in component form:

$$\bar{\mathbf{V}} \cdot \nabla \bar{u} - f\bar{v} + \frac{1}{\bar{\rho}}\frac{\partial \bar{p}}{\partial x} = -\epsilon \bar{u} \qquad (1a)$$

$$\bar{\mathbf{V}} \cdot \nabla \bar{v} + f\bar{u} + \frac{1}{\bar{\rho}}\frac{\partial \bar{p}}{\partial y} = -\epsilon \bar{v} \qquad (1b)$$

where the overbar denotes the climatological mean, and the time tendency and transient horizontal advection terms have been neglected. The object of this study is to determine (i) how well linear drag approximates the vertical eddy stress term over the tropical oceans, and (ii) how well a single ϵ characterizes the eddy stress term over a large domain (i.e., the tropical Pacific), in keeping with the simple formulation of this term in the studies discussed in the Introduction.

3. Data

The monthly mean surface wind and sea level pressure data used in this study are from Sadler et al.'s (1987) analysis of the 1900–79 long-term mean fields from the Comprehensive Ocean–Atmosphere Data Set (COADS). COADS is an extensive compilation of weather observations from ships of opportunity over the World Ocean (see description by Woodruff et al. 1987). The data are archived by 2° squares. The domain for the analysis is the tropical Pacific Ocean: 20°N–20°S, 130°E–70°W. The data have been smoothed with a 1–2–1 filter in both zonal and meridional directions.

The climatological mean surface wind and sea level pressure fields for December–February and June–August are shown in Fig. 1.

4. Results

a. Determination of linear damping coefficients

Figure 2a is a scatterplot of the sum of the pressure gradient, Coriolis, and advective forces in the x direction [e.g., the left-hand side of Eq. (1a)] versus the zonal component of the wind for each 2° square over

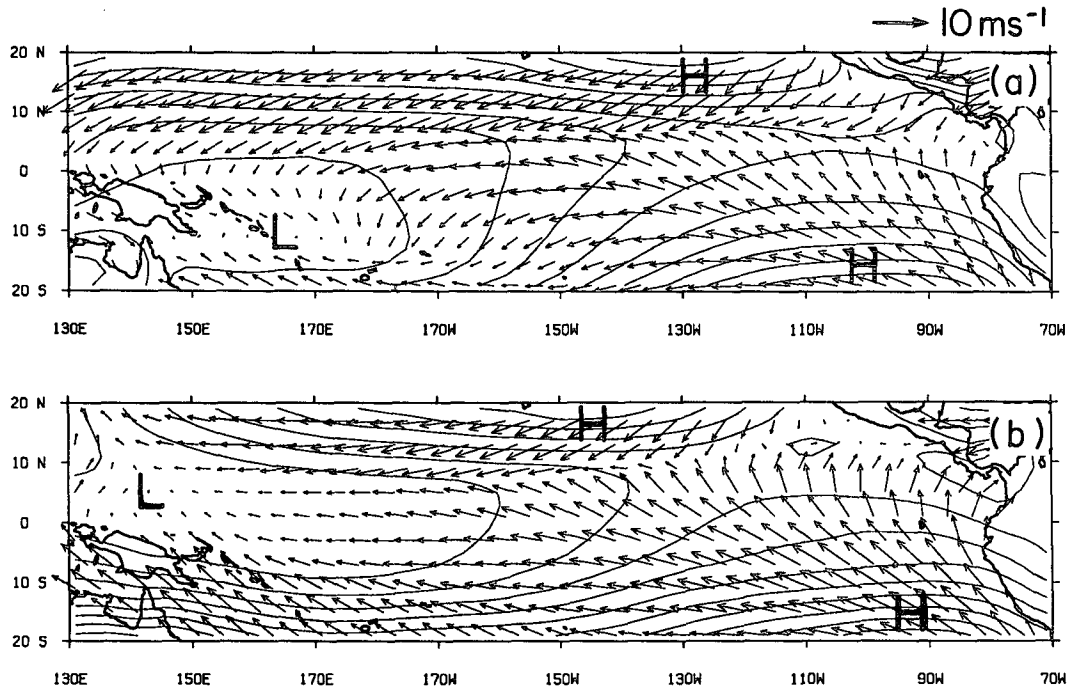

FIG. 1. Climatological-mean surface wind and sea level pressure fields from COADS for (a) December–February and (b) June–August. The pressure fields are contoured every 1 mb. Only every other wind vector is shown. The fields have been smoothed with a 1–2–1 filter in both the zonal and meridional directions.

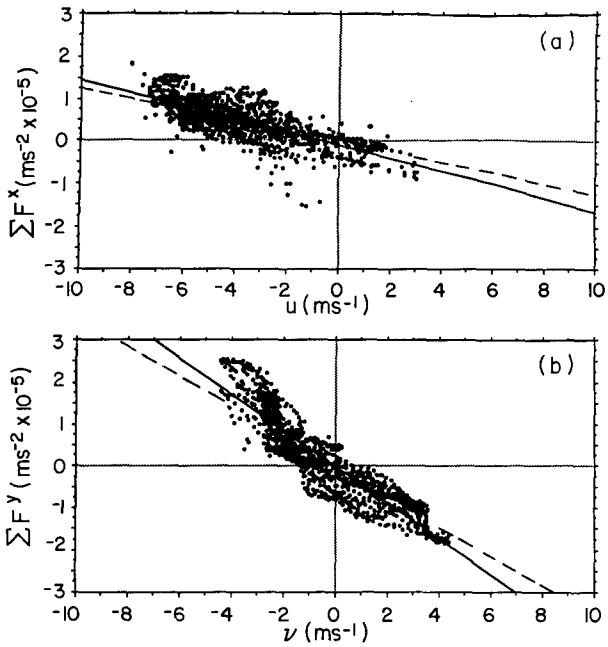

FIG. 2. (a) Scatterplot of the sum of the pressure gradient, Coriolis, and nonlinear advection terms in the x direction vs the zonal component of the wind for each 2° square over the domain 20°N–20°S, 130°E–70°W during December–February. Dashed (solid) line indicates the linear least-squares regression curve that is (is not) constrained to intersect the origin. (b) As in (a) but for the sum of the forces in the y direction vs the meridional component of the wind. The slopes of the regression lines in (a) and (b) determine the damping coefficients for the zonal and meridional wind components, respectively.

the domain 20°N–20°S, 130°E–70°W for the December–February season. The pressure gradient and advection terms were computed using centered finite differences. Similarly, Fig. 2b shows the scatterplot of the sum of the forces in the y direction [e.g., the left-hand side of Eq. (1b)] versus the meridional component of the wind. The slopes of the linear least-squares regression curves in Fig. 2 determine the damping coefficient ϵ. Figure 2 shows that there is a close linear relationship between the sum of the forces and wind speed in both the zonal and meridional directions (correlation coefficients are .77 for Fig. 2a and .88 for Fig. 2b). (A correlation coefficient greater than .25 in magnitude is significant at the .01 level based on a one-tailed t test, taking into account the spatial autocorrelation in the data.) In other words, the linear drag approximation appears to fit the data quite well. Unexpectedly, however, the slopes of the regression lines are significantly different: 1.6×10^{-5} s^{-1} for Fig. 2a and 4.2×10^{-5} s^{-1} for Fig. 2b. If we denote ϵ^x (ϵ^y) as the damping coefficient for the zonal (meridional) wind, then $\epsilon^x = (0.7 \text{ days})^{-1}$ and $\epsilon^y = (0.3 \text{ days})^{-1}$: the damping time is more than twice as fast for v than for u.

Scatterplots were computed for the other seasons. The results, summarized in Table 1a, show that for each season ϵ^y is ~2–3 times faster than ϵ^x. In each case, the damping coefficients are associated with high correlations, indicating that a linear drag law is a good fit to the data.

The regression lines in Fig. 2 and Table 1a intersect the zonal wind axis at ~ -1 m s^{-1} and the meridional wind axis at ~0 m s^{-1}. In other words, when the sum of the pressure gradient, Coriolis, and advective forces in the x direction is zero, the zonal wind speed is significantly different from zero. (A 1 m s^{-1} intercept is significantly different from zero at the .01 level based on a one-tailed t test, taking into account the spatial autocorrelation in the data.) We have computed alternative least-squares regression lines that are constrained to intersect the origin, in keeping with our assumption that linear drag damps the wind to zero. The damping coefficients and associated correlation coefficients obtained from these regression lines are listed in Table 1b for each season. The results show that ϵ^y is ~2.5–4 times faster than ϵ^x in all seasons. The associated correlation coefficients are well above the .01 significance level, although they are somewhat lower than those for the regression lines that are not constrained to intersect the origin.

A similar analysis was performed on the output from a 30-year run of the Geophysical Fluid Dynamics Laboratory (GFDL) General Circulation Model, in which the sea surface temperatures (SSTs) were constrained to follow the observed SSTs during 1950–79 (the so-called GOGA experiment; see Lau and Nath 1990). The model has nine sigma levels and uses spherical harmonics in the horizontal, with rhomboidal truncation at 15 wavenumbers (corresponding to a grid resolution of approximately 4.5° latitude × 7.5° longitude). The vertical eddy stress term is computed according to

$$\frac{\partial}{\partial \sigma}\left(K \frac{\partial \mathbf{V}}{\partial \sigma}\right)$$

where K, the eddy viscosity, is a function of stability and wind shear; the remaining physics are described in Lau and Nath (1990). The December–February 30-year mean wind and pressure fields at the lowest model level ($\sigma = .99$) are in close agreement with observations. The other seasons from the model run were not examined.

Figure 3a is a scatterplot between the frictional stress term in the x direction versus the zonal component of the wind at the lowest model level for the region 20°N–20°S, 130°E–70°W in December–February; similarly, Fig. 3b is a scatterplot between the frictional stress term in the y direction versus the meridional component of the wind. Note that the frictional term is taken directly from the model, not evaluated as a residual in the momentum balance. There is a strong linear relationship between the stress term and wind strength in both the zonal and meridional directions, as evidenced by the high correlation coefficients associated with the linear least-squares regression lines (.86 for u and .91 for v).

TABLE 1a. Damping coefficients (in days) and associated correlation coefficients (ρ) and wind offsets (m s^{-1}) for the surface wind field over the tropical Pacific Ocean (20°N–20°S, 130°E–70°W), determined from a linear least-squares regression of the sum of the pressure gradient, Coriolis, and advection terms vs wind speed. ϵ^x (ϵ^y) denotes the damping coefficient for the zonal (meridional) wind component. u (v) offset denotes the zonal (meridional) wind speed when the sum of the mean pressure gradient, Coriolis, and advection terms is zero. See text for explanation.

	$(\epsilon^x)^{-1}$ (d)	ρ	u offset (m s^{-1})	$(\epsilon^y)^{-1}$ (d)	ρ	v offset (m s^{-1})
Dec–Feb	.74	*.76*	−0.7	.27	*.91*	−0.1
Mar–May	.69	.77	−1.1	.23	.93	0.1
Jun–Aug	.61	.82	−1.4	.24	.88	0.5
Sep–Nov	.56	*.86*	−1.4	.28	*.86*	0.3
Average	.64	—	−1.2	.25	—	0.2

The damping coefficients for the model [ϵ^x = (0.6 days)$^{-1}$ and ϵ^y = (0.3 days)$^{-1}$] are in excellent agreement with observations. If the least-squares regression lines in Fig. 3 are constrained to intersect the origin, then the damping coefficients for the zonal (meridional) wind become ϵ^x = (0.9 days)$^{-1}$ and ϵ^y = (0.25 days)$^{-1}$: again, in excellent agreement with observations.

In summary, parameterizing the vertical eddy stress gradient in the surface momentum balance as a linear dissipation of kinetic energy results in substantially faster damping times for the meridional wind than for the zonal wind over the tropical Pacific Ocean, in both observations and a GCM.

In addition to the momentum balance, the assumption of linear drag was evaluated for the vorticity and divergence equations. The results (not shown) indicate that the damping coefficient for vorticity is similar to that for the zonal wind, while the damping coefficient for divergence is similar to that for the meridional wind. These results are consistent with the fact that the zonal component of the near-surface flow is mainly rotational, whereas the meridional component is mainly divergent (not shown), as may be seen qualitatively by comparing the angle between the surface wind vectors and the isobars in Fig. 1. Similar results are found for the GCM.

b. Wind simulations from observed pressure fields

1) LINEAR BALANCE

How well can the surface winds be reconstructed from the observed sea level pressure field using the damping coefficients determined above? Our first approach was to solve the linear time-mean momentum equations with friction parameterized as $[-\epsilon^x(u-u_0), -\epsilon^y(v-v_0)]$, where u_0 and v_0 are the wind components when the sum of the mean forces is zero (the wind offsets in Table 1a). In this case, the solutions for u and v become

$$u - u_0 = \left[\epsilon^y\left(\frac{-1}{\rho}\frac{\partial p}{\partial x}\right) + f\left(\frac{-1}{\rho}\frac{\partial p}{\partial y}\right)\right]\Big/(f^2 + \epsilon^x\epsilon^y)$$

$$v - v_0 = \left[-f\left(\frac{-1}{\rho}\frac{\partial p}{\partial x}\right) + \epsilon^x\left(\frac{-1}{\rho}\frac{\partial p}{\partial y}\right)\right]\Big/(f^2 + \epsilon^x\epsilon^y).$$

TABLE 1b. As in (a) but for linear least-squares regression curves constrained to intersect the origin.

	$(\epsilon^x)^{-1}$ (d)	ρ	$(\epsilon^y)^{-1}$ (d)	ρ
Dec–Feb	.91	*.62*	.31	*.78*
Mar–May	.93	*.57*	.23	*.74*
Jun–Aug	.95	*.52*	.37	*.57*
Sep–Nov	.95	*.51*	.38	*.63*
Average	.94	—	.32	—

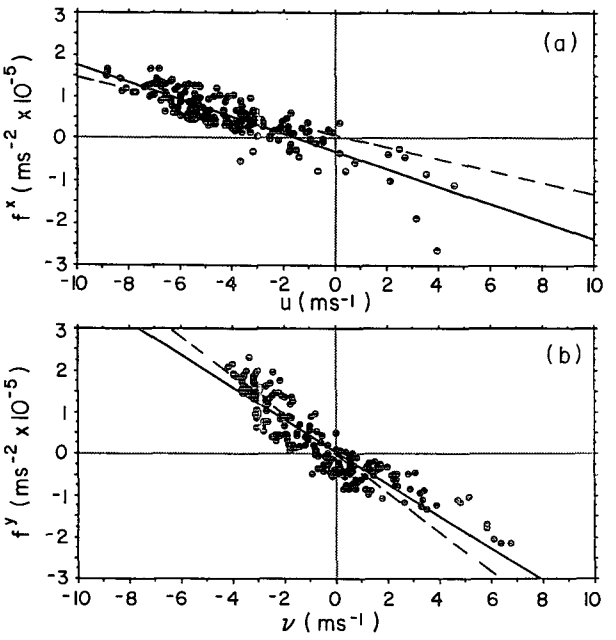

FIG. 3. (a) Scatterplot of the frictional stress term in the x direction vs the zonal component of the wind from the lowest model level of the 30-year GCM climatology for the domain 20°N–20°S, 130°E–70°W during December–February. Dashed (solid) line indicates the linear least-squares regression curve that is (is not) constrained to intersect the origin. (b) As in (a) but for the frictional stress term in the y direction vs the meridional component of the wind. The slopes of the regression lines in (a) and (b) determine the damping coefficients for the zonal and meridional wind components, respectively.

Wind solutions were calculated for values of the damping coefficients and wind offsets obtained from (i) the least-squares regression lines that are not constrained to intersect the origin and (ii) those that are.[1] In both sets of simulations, the average of the seasonal values of the damping coefficients and wind offsets (listed in Table 1) are used, since the differences among the seasons are small and probably due to sampling variations. Pressure gradients were approximated by centered finite differences. Air density was taken as a constant (1.15 kg m^{-3}); it varies by only a few percent over the domain of interest.

Figure 4 shows (a) the observed wind field, (b) the calculated wind field using the damping coefficients and wind offsets from the regression lines that are not constrained to intersect the origin [e.g., $\epsilon^x = (0.64\ \text{d})^{-1}$, $\epsilon^y = (0.25\ \text{d})^{-1}$, u offset $= -1.2$ m s^{-1}, v offset $= 0.2$ m s^{-1}], and (c) the observed–calculated vector wind differences for December–February. The calculated and observed winds show good agreement over the regions occupied by the northeast and southeast trade winds; the largest differences occur over the central equatorial Pacific, where the calculated winds are too weak compared to the observations, and in the vicinity of the South Pacific convergence zone, where the mean winds are relatively light. The average gridpoint rms difference between the calculated and observed wind fields is 1.4 m s^{-1} for u and 0.7 m s^{-1} for v. The rms errors near the equator (6°N–6°S) are 1.6 m s^{-1} for u and 0.9 m s^{-1} for v. Figure 4d shows the December–February observed − calculated wind differences using the damping coefficients from the regression lines that are constrained to intersect the origin [e.g., $\epsilon^x = (0.94\ \text{d})^{-1}$, $\epsilon^y = (0.32\ \text{d})^{-1}$]. The error pattern is similar to that in Fig. 4c, but the magnitude of the zonal wind errors are ~0.4 m s^{-1} larger. The rms errors in Fig. 4d are 1.7 m s^{-1} for u and 0.8 m s^{-1} for v for the full domain, and 2.1 m s^{-1} for u and 0.8 m s^{-1} for v for 6°N–6°S. When wind simulations are performed for the GCM output, a similar pattern of errors is obtained (not shown).

Figure 5 shows the linear wind simulations for June–August. As in December–February, the northeast and southeast trades are well simulated, but the winds in the equatorial zone are weaker than observed and the easterly component of the flow south of 15°S is stronger than observed (Fig. 5c). When damping coefficients from the regression lines constrained to intersect the origin are used (Fig. 5d), the same pattern of errors is obtained but the zonal wind differences are larger. The rms errors in Fig. 5c are 1.3 m s^{-1} for u and 0.9 m s^{-1} for v for the full domain, and 1.4 m s^{-1} for u and 1.1 m s^{-1} for v for 6°N–6°S. The rms errors in Fig. 5d are 1.9 m s^{-1} for u and 1.0 m s^{-1} for v for the full domain, and 2.3 m s^{-1} for u and 1.0 m s^{-1} for v for 6°N–6°S.

Previous studies have computed surface winds from observed sea level pressure fields using equal damping coefficients for u and v (cf. Murphree and Van den Dool 1988; Zebiak 1990). It is therefore of interest to compare the wind fields simulated with equal and unequal damping coefficients. Figure 6 shows the December–February observed–calculated wind vector differences using $\epsilon^x = \epsilon^y = (0.48\ \text{d})^{-1}$ (the average of the damping times for the zonal and meridional winds when the regression lines are constrained to intersect the origin). This choice of equal damping coefficients results in excessively strong meridional winds, both compared to observations and compared to the results with unequal damping coefficients. [Murphree and Van den Dool (1988) also found their simulated meridional wind field to be too strong, even in a nonlinear solution, and Zebiak (1990) obtained excessive wind divergence in his simulation.] The rms differences over the domain are 1.7 m s^{-1} for u and 1.8 m s^{-1} for v. Hence, the surface wind field (the meridional component in particular) is more realistically simulated with $\epsilon^y > \epsilon^x$ than with $\epsilon^x = \epsilon^y$. This result holds for the other seasons and for simulations in which the damping times and wind offsets are determined from the regression lines that are not constrained to intersect the origin (not shown).

2) Nonlinear balance

The importance of the nonlinear terms is evaluated by 1) comparing the drag coefficients computed from the linear and nonlinear momentum equations, and 2) solving the nonlinear momentum equations for the winds using an iterative technique.

Table 2 summarizes the seasonal damping coefficients obtained from the least-squares regression lines that are constrained to intersect the origin for both linear and nonlinear balances. The nonlinear terms alter the damping coefficients by less than 15% in all seasons, and by ~5% for the annual average. This result is also true for the regression lines that are not constrained to intersect the origin (not shown).

The wind field was simulated from the observed pressure field using the nonlinear momentum balance [Eqs. (1a) and (1b)] with friction parameterized as $(-\epsilon^x u, -\epsilon^y v)$ (i.e., the damping coefficients were obtained from the regression lines that intersect the origin). The solution was found using an iterative technique. The first-guess solution was the wind field obtained from the linear momentum balance. The nonlinear advection terms were then calculated from this wind solution. These advective terms were smoothed in the zonal and meridional directions with two passes of a 1–2–1 filter to eliminate small-scale features that make the solution unstable, added to the pressure gradient term as an additional forcing, and a

[1] Since the damping coefficients determined from linear and nonlinear (e.g., advection terms included) balances differ by only ~5% (see next section), the values from the nonlinear balance have been used to calculate linear wind solutions.

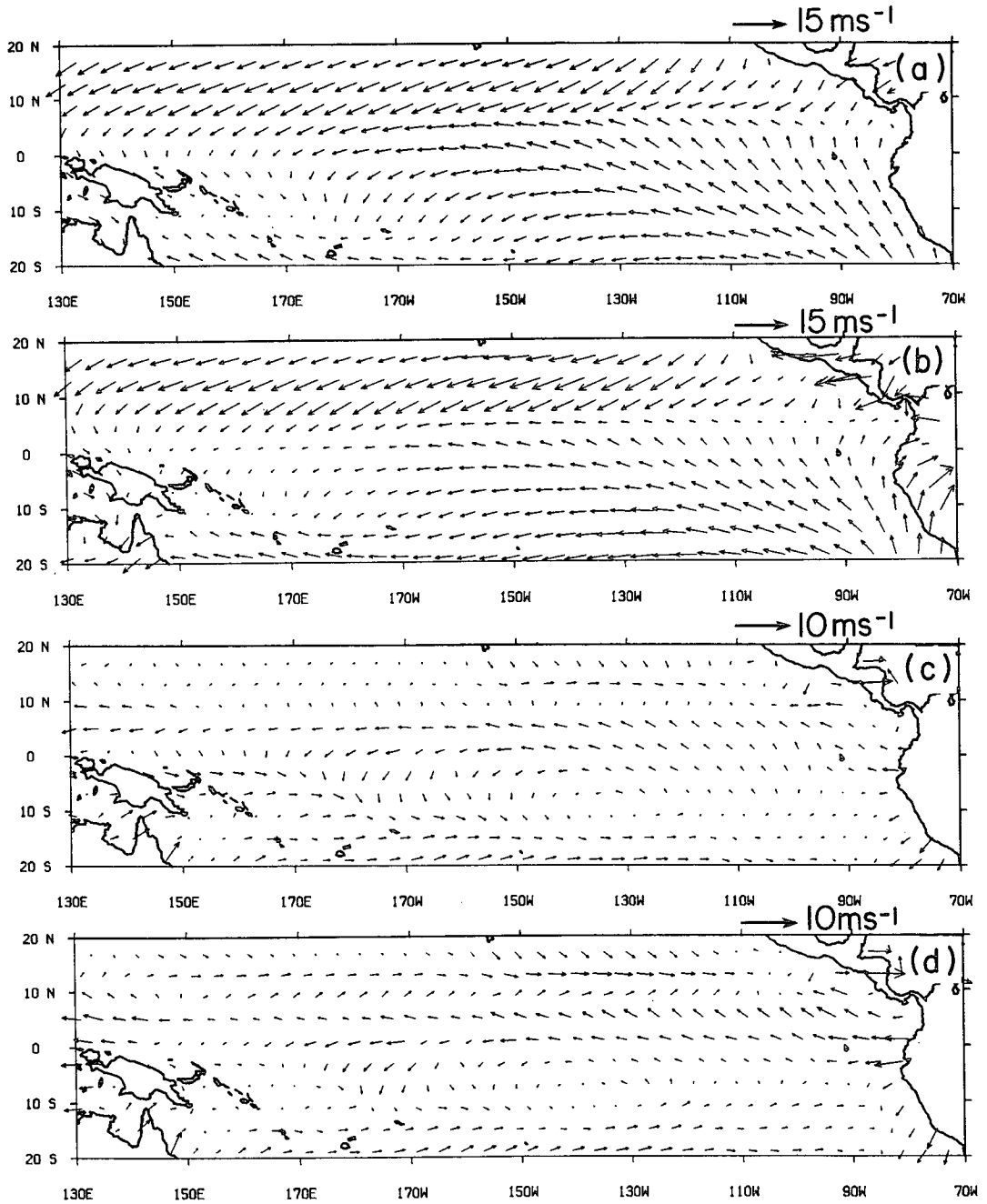

FIG. 4. (a) Observed, (b) calculated, and (c) observed–calculated vector winds for December–February. The winds in (b) and (c) were calculated from the observed sea level pressure field using a linear balance with the damping coefficients and intercepts determined from linear least-squares regression lines not constrained to intersect the origin [$\epsilon^x = (0.64\ \text{d})^{-1}$, $\epsilon^y = (0.25\ \text{d})^{-1}$, u intercept $= -1.2\ \text{m s}^{-1}$, v intercept $= 0.2\ \text{m s}^{-1}$]. (d) Observed–calculated vector winds using a linear balance with the damping coefficients determined from linear least-squares regression lines constrained to intersect the origin [$\epsilon^x = (0.94\ \text{d})^{-1}$, $\epsilon^y = (0.32\ \text{d})^{-1}$]. Note the different wind vector scales in (c) and (d) compared to (a) and (b).

new wind solution was found. The final solution was reached when the winds at two successive iterations differed by less than $0.01\ \text{m s}^{-1}$ at all grid points. Eleven (23) iterations were required for convergence for the December–February (June–August) wind fields. Figure 7a shows the nonlinear wind simulation for December–February, using the standard values $\epsilon^x = (0.94\ \text{d})^{-1}$ and $\epsilon^y = (0.32\ \text{d})^{-1}$; Fig. 7b shows the observed–cal-

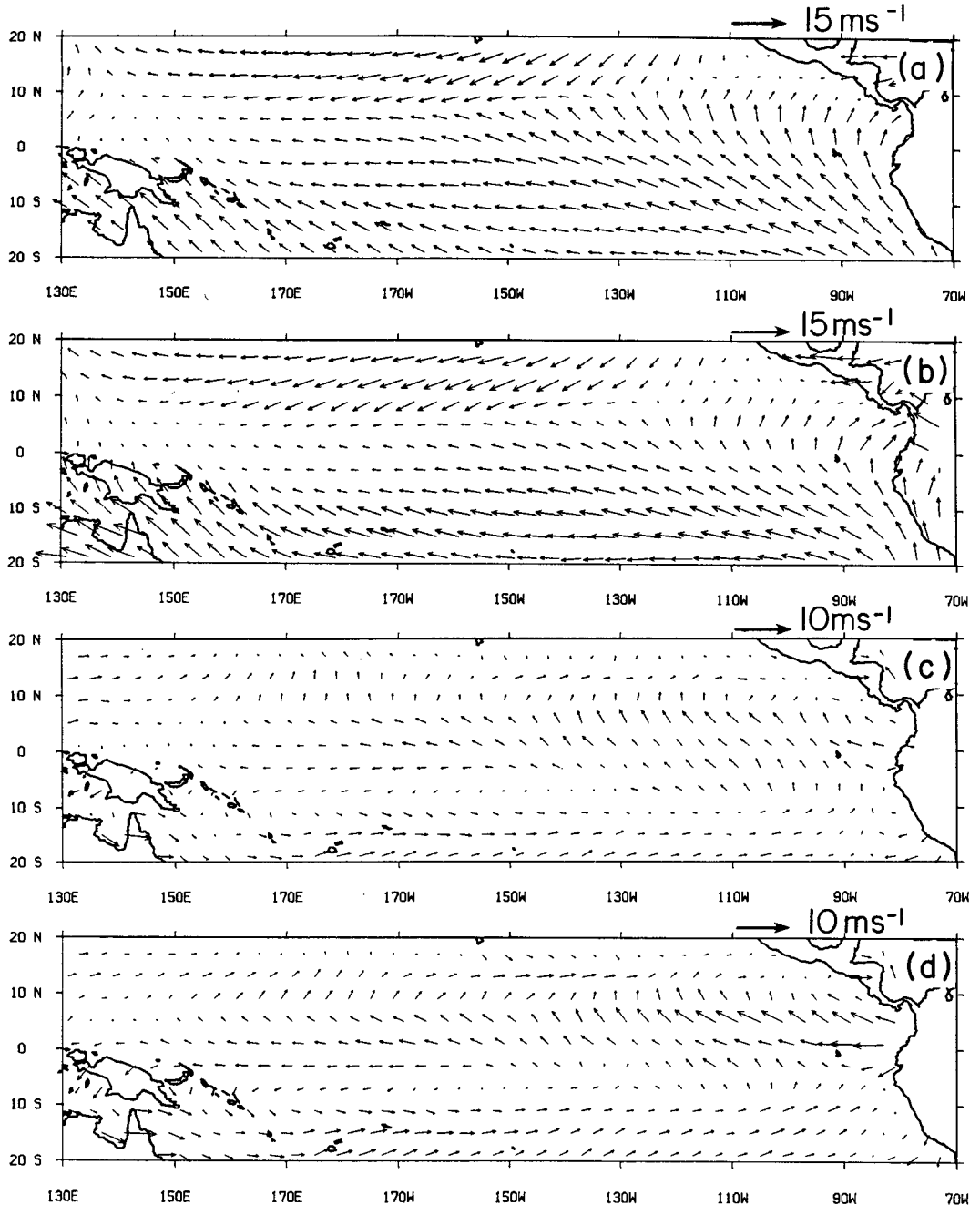

FIG. 5. As in Fig. 4 but for June–August.

culated wind field, and Fig. 7c shows the difference between the nonlinear and linear simulations. The main effect of advection is to strengthen the easterly component of the wind at the southern margin of the northeast trades, off the coasts of Ecuador and Peru, and at the western edge of the equatorial easterlies by ~0.5–1.0 m s^{-1}, bringing the winds in these regions more in line with observations. The rms errors in Fig. 7b are 1.6 m s^{-1} for u and 0.7 m s^{-1} for v for both the full domain and 6°N–6°S. Thus, the nonlinear advection terms improve the zonal wind simulation in the equatorial zone by 0.5 m s^{-1}. Similar results are found for June–August (see Fig. 8). Nonlinear advection has similar effects when damping coefficients and offsets from the regression lines that are not constrained to intersect the origin are used (not shown). Murphree and Van den Dool (1988) and Zebiak (1990) also found that nonlinear advection played only a minor

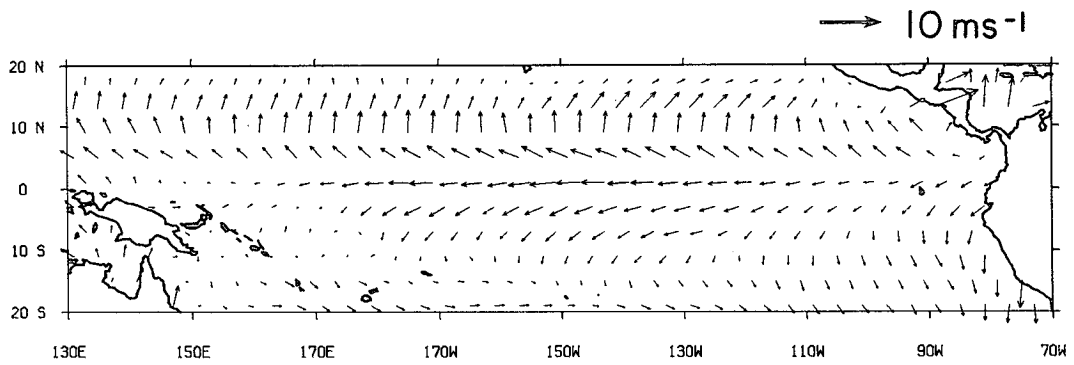

FIG. 6. Observed − calculated vector wind differences for December–February, using a linear balance with $\epsilon^x = \epsilon^y = (0.48\ \text{d})^{-1}$.

role in the surface momentum balance over the tropical Pacific.

The equatorial zonal wind simulation can be improved by another few tenths of meters per second if damping coefficients appropriate for just the equatorial zone are used (as determined from scatterplots for the region 6°N–6°S). The improvement in the equatorial area is, however, at the expense of the higher tropical latitudes (not shown).

5. Discussion

The main finding of this study is that when linear drag is used to parameterize surface friction over the tropical Pacific Ocean, the damping coefficient for the meridional component of the wind is 2–3 times larger than that for the zonal component. A qualitative explanation for why frictional effects are stronger for the meridional wind is offered as follows.

Over the tropical Pacific Ocean, the winds at the top of the planetary boundary layer are predominantly easterly, while those near the surface exhibit a large meridional component (Sadler and Kilonsky 1981; Sadler et al. 1987). Thus, the vertical profiles of u and v in the planetary boundary layer are very different: the zonal wind component tends to have a maximum near the top of the boundary layer (~900 mb), while the meridional wind component tends to have a maximum closer to the surface (Brummer et al. 1974). This suggests that the curvature (second derivative with respect to height) should be larger for v than for u near the surface. In the simplest mixing length model of turbulent transfer (e.g., K constant with height), it is assumed that the vertical eddy stress gradient can be parameterized in terms of the curvature of the mean wind (Fleagle and Businger 1980, pp. 269–273). Thus, the stress gradient should be larger for v than for u near the surface. In a more complete model of turbulent transfer, other factors besides the curvature effect may contribute to the observed differences in the vertical eddy stress gradients.

This analysis has neglected the role of transients in the surface momentum balance. Murphree and Van den Dool (1988) found that nonlinear horizontal advection by transients in the NMC 1000-mb wind analyses preferentially damp the meridional wind relative to the zonal wind. This effect is important only poleward of 20°, however (see their Fig. 13). Thus, it seems unlikely that transients can account for the different damping coefficients in the zonal and meridional directions equatorward of 20° that were found in this study. Furthermore, the damping coefficients from the GFDL model, which agree closely with observations, are obtained from the frictional stress term directly: that is, transients do not enter into the calculation. Thus, nonlinear horizontal advection by transients are not the cause for the different damping coefficients in the model.

TABLE 2. Comparison of damping coefficients obtained from linear and nonlinear balances. ϵ^x (ϵ^y) denotes the damping coefficient for the zonal (meridional) wind component (in days) for the surface wind field over the tropical Pacific Ocean (20°N–20°S, 130°E–70°W), determined from linear least-squares regression curves constrained to intersect the origin.

	$(\epsilon^x)^{-1}$		$(\epsilon^y)^{-1}$	
	Linear (d)	Nonlinear (d)	Linear (d)	Nonlinear (d)
Dec–Feb	0.93	0.91	0.27	0.31
Mar–May	0.95	0.93	0.24	0.23
Jun–Aug	1.02	0.95	0.36	0.37
Sep–Nov	1.05	0.95	0.38	0.38
Average	0.98	0.94	0.30	0.32

6. Conclusions

The purpose of this study was to evaluate the suitability of using linear drag as a proxy for the vertical eddy stress term in the surface momentum balance over the tropical Pacific Ocean. The linear drag pa-

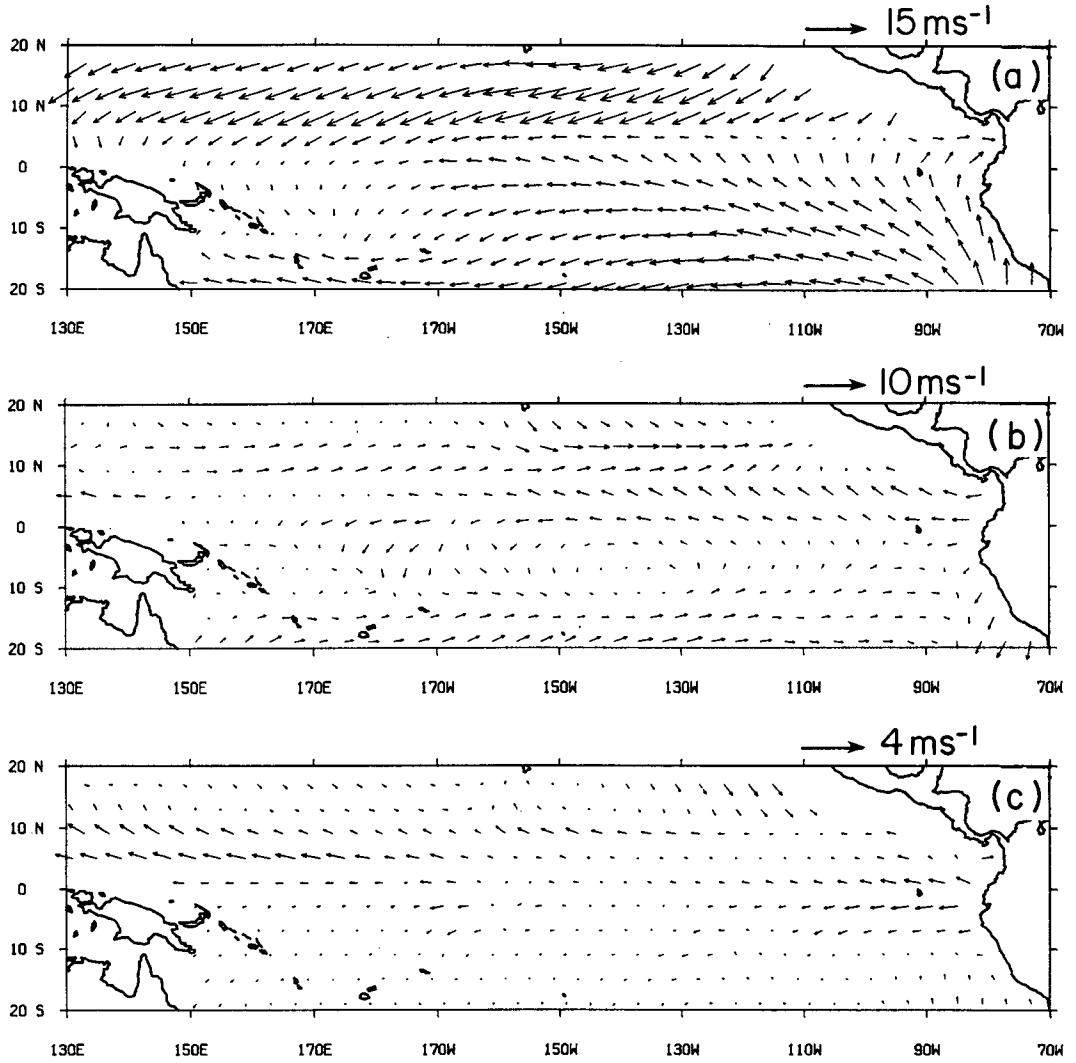

FIG. 7. (a) December–February winds calculated from the observed sea level pressure field using a nonlinear balance with $\epsilon^x = (0.94\ \text{d})^{-1}$, $\epsilon^y = (0.32\ \text{d})^{-1}$. (b) Observed − calculated vector winds. (c) Vector difference between the December–February nonlinear and linear wind solutions. Note the different scales in (a), (b), and (c).

rameterization of momentum dissipation in the planetary boundary layer is widely used in simplified models of the tropical atmosphere (e.g., Matsuno 1966; Gill 1980; Zebiak 1982; Lindzen and Nigam 1987; Neelin 1988), and in numerous observational studies of the surface momentum balance (Hastenrath and Lamb 1978; Egger et al. 1981; Muphree and Van den Dool 1988; Zebiak 1990). When the vertical eddy stress term in the surface momentum balance is formulated as a linear dissipation of kinetic energy, it is found that the damping time scale for the meridional wind is 2–3 times faster than the damping time scale for the zonal wind over the tropical Pacific Ocean, in all seasons. The preceding formulation fits the observations well, especially in the trade-wind regions. Equivalently, the divergent component of the wind is more heavily damped than the rotational component, since the zonal (meridional) component of the trade winds is primarily rotational (divergent).

The tropical Pacific surface zonal (meridional) wind field can be retrieved from the observed sea level pressure field to an accuracy of $\sim 2\ \text{m s}^{-1}$ ($\sim 1\ \text{m s}^{-1}$) using a linear momentum balance with unequal damping coefficients ($\epsilon^y \sim 3\epsilon^x$). With equal damping coefficients, the meridional component of the surface flow is too strong. The inclusion of nonlinear advection improves the zonal wind simulation in limited regions of the northeast trades, equatorial easterlies, and off South America, but only by ~ 0.5–$1.0\ \text{m s}^{-1}$.

The different damping coefficients for the zonal and meridional winds may be, in part, a reflection of the different vertical profiles of u and v in the planetary

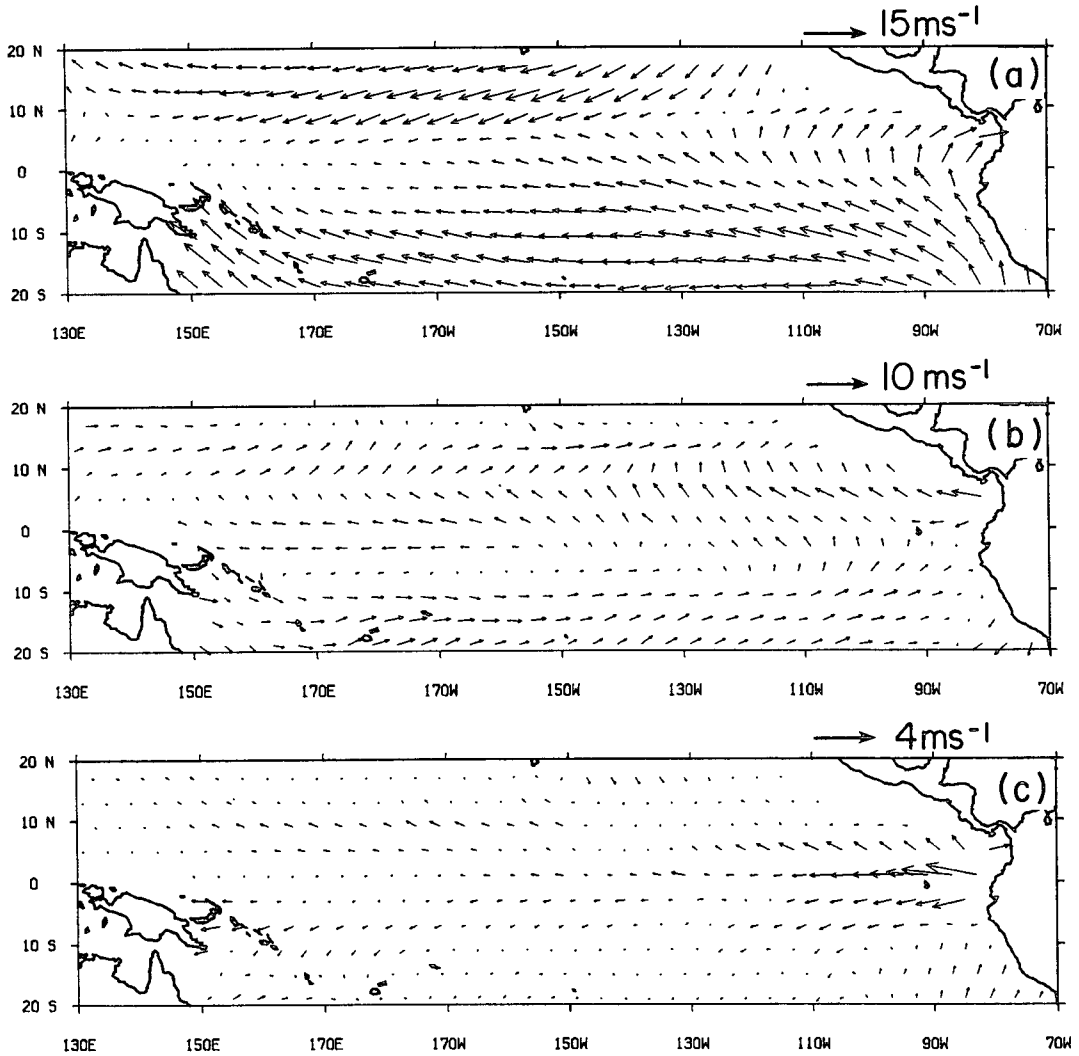

FIG. 8. As in Fig. 7 but for June–August.

boundary layer. While the wind at the top of the tropical boundary layer (~850 mb) is nearly zonal, the surface wind field has a large meridional component. Thus, one may infer that the meridional wind profile is shallower than the zonal wind profile. This leads to larger curvature in v than in u near the surface. It follows that in the simplest case of the vertical eddy stress gradient proportional to the curvature of the mean wind, the stress term should be larger for v than for u, near the surface.

Acknowledgments. I thank Dr. Mingfang Ting for many valuable discussions and for help with accessing the GCM output, and Dr. Maurice Blackmon and Professors John M. Wallace and John A. Young for their encouragement and suggestions. The comments of the reviewers helped to clarify my interpretation of the results. This work was supported by a grant to NOAA's Climate Research Division from the Office of Climate and Global Change.

REFERENCES

Brummer, B., E. Augstein, and H. Riehl, 1974: On the low-level wind structure in the Atlantic trade. *Quart. J. Roy. Meteor. Soc.*, **100,** 109–121.

Egger, J. G., G. Meyers, and P. B. Wright, 1981: Pressure, wind, and cloudiness in the tropical Pacific related to the Southern Oscillation. *Mon. Wea. Rev.*, **109,** 1139–1149.

Fleagle, R. G., and J. A. Businger, 1980: *An Introduction to Atmospheric Physics.* Academic Press, 432 pp.

Gill, A. E., 1980: Some simple solutions for heat-induced tropical circulation. *Quart. J. Roy. Meteor. Soc.*, **106,** 447–462.

Gordon, A. H., and R. C. Taylor, 1975: Computations of surface layer air parcel trajectories and weather on the oceanic tropics. *Int. Indian Ocean Expedition, Meteor. Monogr.* No. 7, University of Hawaii Press, 112 pp.

Hastenrath, S., and P. Lamb, 1978: On the dynamics and climatology of surface flow over the equatorial oceans. *Tellus,* **30,** 436–448.

Lau, N.-C., and M. J. Nath, 1990: A general circulation model study of the atmospheric response to extratropical SST anomalies observed in 1950–79. *J. Climate,* **3,** 965–989.

Lindzen, R. S., and S. Nigam, 1987: On the role of sea surface temperature gradients in forcing low-level winds and convergence in the tropics. *J. Atmos. Sci.,* **44,** 2440–2458.

Matsuno, T., 1966: Quasigeostrophic motions in the equatorial area. *J. Meteor. Soc. Japan,* **44,** 25–43.

Murphree, T., and H. van den Dool, 1988: Calculating winds from time mean sea level pressure fields. *J. Atmos. Sci.,* **45,** 3269–3281.

Neelin, J. D., 1988: A simple model for surface stress and low-level flow in the tropical atmosphere driven by prescribed heating. *Quart. J. Roy. Meteor. Soc.,* **114,** 747–770.

Sadler, J. C., and B. J. Kilonsky, 1981: Trade wind monitoring using satellite observations. *UHMET 81-01,* University of Hawaii, Honolulu, Hawaii.

——, M. A. Lander, A. M. Hori, and L. K. Oda, 1987: *Tropical Marine Climatic Atlas, Vol. 2, Pacific Ocean.* UHMET 87-02, University of Hawaii, Honolulu, Hawaii.

Seager, R., 1991: A simple model of the climatology and variability of the low-level wind field in the tropics. *J. Climate,* **4,** 164–179.

Webster, P. J., 1972: Response of the tropical atmosphere to local, steady forcing. *Mon. Wea. Rev.,* **100,** 518–541.

Woodruff, S. D., R. J. Slutz, R. L. Jenne, and P. M. Steurer, 1987: A comprehensive ocean–atmosphere data set. *Bull. Amer. Meteor. Soc.,* **68,** 1239–1250.

Zebiak, S. E., 1982: A simple atmosphere model of relevance to El Niño. *J. Atmos. Sci.,* **39,** 2017–2027.

——, 1990: Diagnostic studies of Pacific surface winds. *J. Climate,* **3,** 1016–1031.